

## 1 Response to the reviewers

### 2 Review 1

3  
4 **Comment 1:** However, several parts of the methodology section should be further developed and  
5 details should be given about some choices performed. The validity of the satellite remote sensing  
6 imagery and numerical modelling methods followed should be proved to accurately detect and re-  
7 produce the plume dynamics.

8  
9 The description of the methodology followed both through satellite remote sensing imagery and  
10 numerical modelling it is not sufficiently complete and precise to allow their comprehension and  
11 reproduction by other experts and therefore the results are not traceable.

12 Section 2.1: The methods to distinguish the turbid water from the clear sea water should be scien-  
13 tifically and precisely defined to allow the application of satellite remote sensing imagery to plume  
14 detection;

15 **Reply:** Additional information was added to the manuscript in order to make the satellite based re-  
16 sults reproducible and traceable.

17 Two things that were missing and could help the reader are (1) the reference to the software  
18 (BEAM) that was used for image processing and (2) information about the used quality flags for  
19 masking invalid pixels. The missing information is now added to the manuscript. The BEAM, along  
20 with the algorithms in it, is a standard tool/method for MERIS data processing. The relevant infor-  
21 mation necessary for the reproduction of the results is as follows:

22 -Satellite sensor- ENVISAT/MERIS

23 - The database from which MERIS images were acquired- <http://www.coastcolour.org/data/archive/>

24 -Processing algorithm- C2R algorithm is described in detail by Doerfer and Schiller (2007). The  
25 algorithm has been validated in the Baltic Sea region in numerous studies. We added some extra  
26 references to the algorithm.

27 -Projection, resolution information- UTM34, 0.3 km

28 -Software package- BEAM (<http://www.brockmann-consult.de/cms/web/beam/>)

29 -Quality flags that were used in processing- ! 11p\_cc\_land and ! 11b\_invalid and !

30 11p\_cc\_cloud\_shadow and ! case2\_invalid and ! case2\_whitecaps and ! case2\_conc\_oor and !

31 11p\_cc\_glintrisk and ! 11p\_cc\_cloud\_shadow and ! 11p\_cc\_cloud\_buffer and !

32 11p\_cc\_cloud\_ambiguous and ! 11p\_cc\_cloud and ! sunglint and ! 11p\_cc\_snow\_ice

33  
34 **Comment 2:** Section 2.2: It is essential to perform a comparison between satellite imagery results  
35 and observations to prove the adequacy and validity of the methods applied;

36 **Reply:** The in situ measurements of TSM concentrations or optical properties were not conducted at  
37 the time of the study period. Therefore, the algorithm was not directly validated for the specific re-  
38 gion and period. However, the C2R algorithm for the Baltic Sea has been validated in numerous  
39 previous studies (from Bothnia in the north to the Polish coast in the south, and from the Swedish  
40 coast in the west to the Gulf of Finland in the east) (Siitam et al 2014, Attila et al.2013, Vaičiūtė et  
41 al 2012) and its advantages and disadvantages are known. The C2R algorithm has been proven to be  
42 suitable for monitoring of water quality parameters (including TSM).

43 Satellite imagery studies of many river bulges (including Mendes et al. 2014, Horner-Devine et al  
44 2008 etc) have exploited MODIS data, which has been processed with SeaDAS software package  
45 and algorithms. However, it is common knowledge, and has been pointed out also by Goyens et al  
46 (2013), that standard MODIS atmospheric correction algorithms give poor results in the Baltic Sea  
47 compared to other regions of the world ocean. The inaccurate atmospheric correction procedures  
48 impact the retrieval of remote sensing reflectance, IOPs and water quality parameters in the Baltic  
49 Sea from MODIS imagery using standard processing algorithms (including the ones in SeaDAS).  
50 Numerous studies in the Baltic Sea have proved that MERIS is more suitable for water quality mon-  
51 itoring than other sensors (eg. MODIS, Seawifs). This is due to the selection of spectral bands by

1 the MERIS instrument (sufficient spectral resolution in the range of wavelength above 555 nm),  
2 which is designed for monitoring optically complex waters like the Baltic Sea (Gitelson et al. 2009).  
3 The methods referred to in Mendes et al. (2014) and Horner-Devine et al. (2008) exploit SEADAS,  
4 which is not applicable in the Baltic Sea and causes heavy overestimation of water quality param-  
5 eter values. While the analogous atmospheric correction, IOP and water quality parameter retrieval  
6 algorithm for MERIS, the C2R that we used, performs better in the Baltic Sea. Moreover, Mendes  
7 et al. 2014 found the normalized water leaving radiance at band 555nm (SeaDAS) to be the most  
8 suitable for bulge monitoring as it had sufficiently high correlation ( $r=0.56$  for MODIS/Terra and  
9  $r=0.60$  for MODIS/Aqua) with river discharge. In the MERIS studies mentioned above, the TSM  
10 concentrations retrieved with the C2R algorithm from MERIS imagery were correlated with in situ  
11 measurements of TSM concentrations. The corresponding correlation coefficients ( $r$ ) were between  
12 0.72 and 0.87, which is significantly better compared to the Mendes et al (2014) study. Although the  
13 numbers are not comparable one-on-one, they imply that the MERIS-based TSM retrieval represents  
14 TSM variation in the upper layer reasonably well. Thus, the use of C2R algorithm for MERIS im-  
15 age processing over the Baltic Sea region is justified.

16  
17 **Section 2.2:** Why the measurements of Gauja and Lielupe rivers fows were multiplied by 1.05 and  
18 1.87, respectively? How were obtained these numbers? The use of this numbers has to be justified.

19 **Reply:** The coefficients are obtained as a ratio between the whole catchment area of those rivers  
20 and the catchment area of those rivers up to the place/station where the river flow was measured.  
21 Coefficient = whole catchment area / catchment area up to the measured location. Clarification was  
22 added in the revised manuscript.

23  
24 **Section 2.3:** model calibration and validations results must be presented through comparison with  
25 in situ field data, and the model predictions accuracy has to be quantified; additionally, the compari-  
26 son should prove the models accuracy in simulating the local river plumes dynamics;

27 **Reply:** A new section (2.4 Model validation) was added to the revised manuscript.

28  
29 **Section 2.3:** The model TSM input used for the river discharges should be characterized (Realistic  
30 values? Real values measured in situ? Where?)

31 **Reply:** TSM concentration in the river water was set to a unit value, as we do not have measure-  
32 ments of TSM concentrations in the river. The passive tracer was released to the GoR as Daugava  
33 River load of TSM being proportional to the Daugava River run-off starting from 20 March. Thus,  
34 the load is equal to TSM concentration multiplied with river run-off. The latter varying in time, as  
35 measured. We added clarification in the revised manuscript.

36  
37 **Section 3.1:** the analysis presented should start before the plume establishment (maybe on #17th  
38 March) in order to allow the understanding of the plume dynamics in response to the high freshwa-  
39 ter discharge event;

40 **Reply:** A 3-day spin-up period with a realistic salinity field and a linear increase of river run-off  
41 from zero to measured river run-off value on 20 March 2007 was used before including wind forc-  
42 ing on 20 March. Thus, we reached the peak value of freshwater discharge. During the spin-up peri-  
43 od the wind speed was high, i.e. between 6 and 12 m/s (Fig. 2). As shown in Section 3.2, the wind  
44 of 4 m/s affects the bulge considerably, so we may expect that much stronger wind would mix river  
45 water with surrounding water in natural conditions. The satellite image on 20 March shows a much  
46 smaller plume and bulge than on the following images (Fig. 4a). Therefore, we suggest that this  
47 plume corresponds mainly to the initiation of the plume at midnight between 19 and 20 March  
48 when wind speed decreases from 6 to 2 m/s. Checking the sequence of tracer spreading in the nu-  
49 merical model showed that the bulge showing on the satellite image of 20 March (Fig. 4a) was de-  
50 stroyed by moderate wind of 5-6 m/s on 24 March (Fig. 2b). Upwelling favourable wind has sig-  
51 nificant effect on the bulge evolution, as shown with additional numerical experiments with con-  
52 stant wind from different directions (Fig.6 in revised ms). The plume on 26 March was the result of

1 the reset of the river plume on 24 March. The bulge analysed in the present study started to develop  
2 after March 24 at 05:00 and existed for the following 7-8-days. In order to retain the focus of the  
3 paper, we concentrated on a single long-lasting bulge evolution event.

4  
5 **Section 3.3:** Why was used an ambient water salinity of 6? Please justify this assumption;

6 **Reply:** Based on the measurement study carried out between 1973–1995 in the GoR by Raudsepp  
7 (2001), long term average value for the salinity in the central GoR was about 6 (Raudsepp 2001,  
8 Figure 2b). We added T/S profile, adopted from Raudsepp (2001), to the Figure 1 in revised ms.

9  
10 **Section 3.3:** simulations of rivers discharge into a homogeneous GoR with an ambient water salin-  
11 ity should also be performed considering idealized winds of growing intensity to analyse  
12 the wind effect in the evolution of the river bulge; without this the discussion and conclusions about  
13 the wind effect on the river bulge establishment and evolution are not solid;

14 **Reply:** We have made additional simulations with cross-shore and alongshore winds of 2 m/s and 4  
15 m/s. We added paragraph and a figure to the revised manuscript.

16  
17 **Section 3.4:** without comparison with in situ field data it is impossible to prove that  
18 model results are describing the local patterns and physics of the river bulge dynamics; -

19 **Reply:** Comparison of in situ data and model simulation results were made and a new section (2.4  
20 "Model validation") has been added to the revised manuscript.

21  
22 **Section 3.4:** the selection of threshold values based on visual inspection of TSM concentration  
23 maps on the satellite images is subjective and therefore not scientific; moreover, it is not acceptable  
24 that this threshold varied from image to image;

25  
26 **Reply:** There is no established methodology to determine bulge edge. Multiple previous studies  
27 define the bulge edge based on selected constant threshold values. Horner-Devine et al (2006) esti-  
28 mated that a quadratic curve captures the bulge front for the central region but not on the bulge  
29 edges. Therefore, a constant 20% buoyancy contour was chosen as a reference value since isolines  
30 corresponding to lower buoyancy levels reflect too much variability and become difficult to fit.  
31 Gregorio et al. (2011) used reference velocity, 1.7cm/s, to define the coastal current front. Soosaar  
32 et al. (2015) defined the bulge edge to be 10% from the discharge depth.

33  
34 We have removed from the revised manuscript the parts where bulge measures from satellite images  
35 are defined, described, calculated and discussed. We kept the bulge measures calculated from nu-  
36 merical model results. We calculated the bulge boundary with different threshold values. Although  
37 the actual boundary changes, the dynamics of the bulge does not depend on the selected threshold  
38 value. We have added text and modified the Fig 7 in the revised manuscript.

39  
40 **Section 3.4:** methods such as those developed by Horner-Devine et al. (2008) or more recently by  
41 Mendes et al (2014) based on the normalized water-leaving radiance should be developed and ap-  
42 plied for plume detection;

43 **Reply:** The methods referred to in Mendes et al. (2014) and Horner-Devine et al. (2008) exploit  
44 SEADAS, which is not applicable in the Baltic Sea and causes heavy overestimation of water quali-  
45 ty parameter values. While the analogous atmospheric correction, IOP and water quality parameter  
46 retrieval algorithm for MERIS, the C2R that we used, performs better in the Baltic Sea. Moreover,  
47 Mendes et al. 2014 found the normalized water leaving radiance at band 555nm (SeaDAS) to be the  
48 most suitable for bulge monitoring as it had sufficiently high correlation ( $r=0.56$  for MODIS/Terra  
49 and  $r=0.60$  for MODIS/Aqua) with river discharge. In the MERIS studies mentioned above, the  
50 TSM concentrations retrieved with the C2R algorithm from MERIS imagery were correlated with  
51 in situ measurements of TSM concentrations. The corresponding correlation coefficients ( $r$ ) were  
52 between 0.72 and 0.87, which is significantly better compared to Mendes et al. (2014) study. Alt-

1 hough the numbers are not comparable one-on-one, they imply that the MERIS-based TSM retrieval  
2 al represent TSM variation in the upper layer reasonably well. Thus, the use of the C2R algorithm  
3 for MERIS image processing over the Baltic Sea region is justified.

4  
5 We have removed the parts from the revised manuscript where bulge measures from satellite images  
6 are defined, described, calculated and discussed.

7  
8 **Section 3.4:** Why was assumed that the bulge has a circular shape (equation 2)? This should be justified; -  
9

10  
11 **Reply:** Methodology is selected with the aim to maintain consistency with previous river bulge  
12 studies (Horner-Devine, 2009; Horner-Devine et al., 2008; Horner-Devine et al., 2006), where bulge  
13 radius is calculated assuming a circular shape, although the actual bulge is not circular. We have  
14 added clarification to the revised manuscript.

15  
16 Remaining results, discussion and conclusion sections: as the results are all unproven due to the  
17 major flaws previously referred, these sections are purely speculative.

#### 18 **References**

19  
20 Doerffer, R. and Schiller, H.: The MERIS case 2 water algorithm. *International Journal of Remote*  
21 *Sensing*, 28(3-4), 517–535, 2007.

22  
23 Siitam, L., Sipelgas, L., and Uiboupin, R.: Analysis of natural background and dredging-induced  
24 changes in TSM concentration from MERIS images near commercial harbours in the Estonian  
25 coastal sea. *International Journal of Remote Sensing*, 35(18), 6764 - 6780, 2014.

26  
27 Attila, J., Koponen, S., Kallio, K., Lindfors, A., Kaitala, S., and Ylöstalo, P.: MERIS Case II water  
28 processor comparison on coastal sites of the northern Baltic Sea. *Remote Sensing of Environment*,  
29 128, 138-149, 2013.

30  
31 Vaičiūtė, D., M. Bresciani, and M. Bučas. 2012. “Validation of MERIS Bio-Optical Products with  
32 In Situ Data in the Turbid Lithuanian Baltic Sea Coastal Waters.” *Journal of Applied Remote Sensing*  
33 6: 063568-1–063568-20. doi:10.1117/1.JRS.6.063568.

34  
35 Horner-Devine, A.R., Fong, D.A., and Monismith, S.G.: Evidence for the inherent unsteadiness of a  
36 river plume: Satellite observations of the Niagara River discharge., *Limnol. Oceanogr.*, 53, 2731-  
37 2737, 2008.

38  
39 Mendes, R., Vaz, N., Fernández-Nóvoa, D., Silva, J., Decastro, M., Gómez-Gesteira, M., and Dias,  
40 J.: Observation of a turbid plume using MODIS imagery: The case of Douro estuary (Portugal).  
41 *Remote Sensing of Environment*, 154, 127-138, 2014.

42  
43 C. Goyens, C. Jamet, T. Schroeder (2013). Evaluation of four atmospheric correction algorithms for  
44 MODIS-Aqua images over contrasted coastal waters. *Remote Sens. Environ.*, 131, 63-75.

45  
46 Gitelson, A.A., Gurlin, D., Moses, W.J. and Barrow, T. 2009. A bio-optical algorithm for the remote  
47 estimation of the chlorophyll-a concentration in case 2 waters *Environmental Research Letters*  
48 4(4), Article Number: 045003 DOI:10.1088/1748-9326/4/4/045003

49  
50 Raudsepp, U. Interannual and seasonal temperature and salinity variations in the Gulf of Riga and  
51 corresponding saline water inflow from the Baltic Proper. *Nordic Hydrology*, 32 (2), 135–160,  
52 2001.

1  
2 Gregorio, S.O., Haidvogelb, D.B., Thomasa, P.J., Taskinogluc, E.S. and Skeend, A.J.: Laboratory  
3 and numerical simulations of gravity-driven coastal currents: Departures from geostrophic theory.  
4 *Dynamics of Atmospheres and Oceans* 52 (2011) 20– 50, 2011.  
5  
6 Soosaar, E., Hetland, R. D., Horner-Devine, A., Avenir, M. E. and Raudsepp, U.: Offshore spread-  
7 ing of buoyant bulge from numerical simulations and laboratory experiments. In: *IEEE Xplore: Bal-*  
8 *tic International Symposium (BALTIC), 2014 IEEE/OES, 27-29 May 2014, Tallinn Estonia. IEEE,*  
9 *2014*  
10  
11 Horner-Devine, A.R.: The bulge circulation in the Columbia River plume., *Cont. Shelf Res.*, 29,  
12 234-251, 2009.  
13  
14 Horner-Devine, A.R, Fong, D. A., Monismith, S. G. and Maxworthy, T.. Laboratory experiments  
15 simulating a coastal river inflow. *J. Fluid Mech.* 555, 203-232, 2006.  
16  
17

## 1 Review 2

2  
3 **Comment 1.** The paper describes many details of the observation and simulation that without  
4 enough explanation of why these features occur. It should be more concise and deliver a more fo-  
5 cused “story” the readers.

6 **Reply:** We have tried to rewrite the paper in a more concise manner and to give more explanations.  
7

8 **Comment 2.** It is mentioned in the paper that the tidal oscillation is small in the study region, thus  
9 tide forcing is not considered, however an additional case with tide forcing should be considered to  
10 approve that the tidal influence on the river bulge is negligible, as many studies show that tide-  
11 induced mixing have significant effect on the structure of the river plume (Chao, 1990; MacCready  
12 et al., 2009; Zu et al., 2014)

13  
14 **Reply:** There is a big difference in the magnitude of tidal oscillation between noted studies and  
15 tides in the Baltic Sea and the GoR. MacCready et al., (2009) study is based on Columbia River and  
16 Zu et al. (2014) is looking at a Pearl River Estuary in South China Sea where tidal oscillations are in  
17 the range of 2-6m). In the Baltic Sea, tides vary in range 1-10 cm, which is mentioned in the text. In  
18 comparison with other forcing acting on the river bulge (wind, variation in river flow), tides in the  
19 GoR are marginal.

20 There are no studies on the effect of tidal mixing to the overall vertical mixing in the Baltic Sea.  
21 Lilover has calculated the contribution of the tidal shear on the gradient Richardson number in the  
22 Gulf of Finland. Results show that tidal contribution is about 10-20% if  $Ri = 1$  (personal communi-  
23 cation). Our ten month long measurements of currents in the GoR with ADCP show that tidal con-  
24 stituents are negligible in the current velocity spectrum (unpublished).  
25

26 **Comment 3.** By using the term balance on a certain time, the paper concludes that geostrophic bal-  
27 ance is valid for the entire mid-field of the bulge, which is different with previous results. However,  
28 time series of the term balance should be presented to approve that the conclusion is universal here,  
29 and is not an occasional event.

30 **Reply:** We calculated the time series of spatially averaged momentum balance terms, Eq. (3), for an  
31 ideal and real bulge and added a paragraph and Fig. 9 to the revised manuscript.  
32

33 **Comment 4.** As many results are based on the model simulation, more detailed description of the  
34 model set up is needed, (i.e. numerical scheme, physical forcing, open boundary conditions ...)

35 **Reply:** Additional information was added to the model description section in the revised manu-  
36 script.  
37

38 **Comment 5.1** On page 4, at line 20-28, the author should add some short statement about the circu-  
39 lation in the Baltic Sea.

40 **Reply:** We assume that the reviewer meant the Gulf of Riga. As the GoR is a nearly closed gulf that  
41 connects with the Baltic Sea through two narrow straights, circulation in the Baltic Sea does not  
42 have relevant effect on the circulation in the GoR. We added a paragraph in the revised ms.  
43

44 **Comment 5.2** The observed representative T/S profile should be plotted in Figure 1.

45 **Reply:** T/S profiles were added to the Figure 1 in the revised ms.  
46

47 **Comment 6.** On page 6, at line 20-21, the Baltic Sea has two large straits (Irbe Strait and Virtsu  
48 Strait) and these strait has important effects on the circulation in the Baltic Sea, why the model use  
49 the closed boundaries?

50 **Reply:** We assume that the reviewer meant the Gulf of Riga. In the study by Soosaar et al. (2014) it  
51 is quantified that in case of over a month long simulation correlation between circulation created in

1 a closed and open boundary, simulation has  $R^2 = 0.93$ . Differences were located in the immediate  
2 proximity of the straits. Our simulation concentrated on the south-east part of the GoR where the  
3 influence is negligible over a time period of two weeks, i.e. the model simulation period. An ex-  
4 planatory text is added to the revised ms.

5  
6 **Comment 7.** On page 7, at line 5-6, the spin-up time of the model only 3 days. It seems too short?

7 **Reply:** A 3-day model spin-up time was used to smooth out small-scale spatial salinity discontinu-  
8 ities due to interpolation and to allow smooth input of fresh water from rivers to ambient saline wa-  
9 ter. As initial salinity fields were interpolated from the 1 nautical mile simulation for the Baltic Sea  
10 (Maljutenko and Raudsepp 2014) on 20 March 2007, we expect that the density field is consistent  
11 with hydrodynamical and meteorological conditions on 20 March 2007. Therefore, we expect that a  
12 3-day geostrophic adjustment is sufficient to spin-up the velocity field. Using longer spin-up with-  
13 out wind forcing would result in considerably different salinity/density fields that were characteris-  
14 tic for 20 March 2007.

15  
16 **Comment 8.** On page 12, at line 5, „the pulsation of the actual bulge" should be „the pulsation of  
17 the real bulge".

18 **Reply:** Corrected.

19  
20 **Comment 9.** On page 12, at line 5-10 (shown in Figure 5). For ideal bulge, when bulge diameter  
21 increased, bulge mean depth increased. The statement “when bulge diameter increased, bulge mean  
22 depth decreased and vice versa.” why?

23 **Reply:** We suggest that the fresh water volume in the bulge is roughly conserved. Therefore, the  
24 bulge depth responds to lateral bulge fluctuations. As the bulge area extends, the bulge depth de-  
25 creases and vice versa. We do not have detailed explanation and future study is needed to have a  
26 solid answer, which we think is beyond the aim of this paper. Therefore, we like to keep it as a noti-  
27 fication without any speculation provided in the text.

28  
29 **Comment 10.** On page 14, at line 5-15, The real simulation gave  $r_b \sim t^{0.50 \pm 0.04}$  while the ideal simula-  
30 tion gave  $r_b \sim t^{0.28 \pm 0.0}$ . And the satellite remote sensing gave  $r_b \sim t^{0.31 \pm 0.23}$ . Why is the evolution of the  
31 bulge in the ideal simulation more similar to that in the satellite remote sensing?

32 **Reply:** The approximation of the growth rate of the bulge radius from satellite remote sensing has  
33 large uncertainty (0.23) as there are too few satellite images available. We have removed from the  
34 revised manuscript the parts where bulge measures from satellite images are defined, described,  
35 calculated and discussed. Thus, the approximation,  $r_b \sim t^{0.31 \pm 0.23}$ , was removed from the revised  
36 manuscript.

37  
38 **Comment 11.** On page 15, at line 24, “one km” should be “1km”

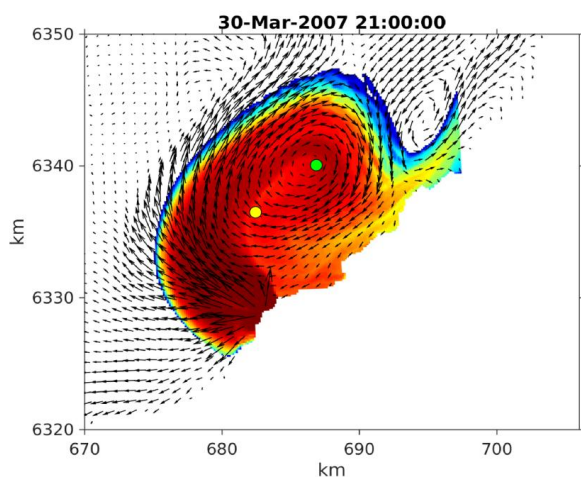
39 **Reply:** Corrected.

40  
41 **Comment 12.** On page 16, at line 24, the bulge centre should be defined using geometric mean po-  
42 sition of the distribution of the tracer concentration. The reason is that when ambient current over-  
43 rode bulge circulation, the bulge centre was not defined using with closed streamlines, although the  
44 bulge still existed if we look at the distribution of the tracer concentration.

45  
46 **Reply:** The bulge centre is defined from the velocity field because we calculate momentum balance  
47 and movement of the bulge centre. Momentum balance is calculated in a cylindrical coordinate sys-  
48 tem where the origin of coordinates is located at the point where angular and radial velocity compo-  
49 nents are zero. This definition is consistent with previous studies that address momentum balance  
50 calculation inside the bulge and movement of the bulge centre (Nof and Pichevin 2001; Horner-  
51 Devine et al. 2006; Horner-Devine 2009).

1 We have calculated the bulge centre as a geostrophic mean position of the distribution of the tracer  
2 concentration and from the velocity field for the real bulge (enclosed with answers to the reviewer,  
3 Fig. rv2.1). In the case of geometric mean, the bulge centre is close to the river mouth, but 5 km  
4 from the bulge centre defined from the velocity field. Placing the origin of cylindrical coordinates in  
5 the geometric mean positions and calculating the momentum balance hampers the interpretation and  
6 comparison of our results with previous studies. Over the course of the model simulations, the centres  
7 of ideal and real bulge defined using geometric mean remain closer to the river mouth than the  
8 centres from the velocity field (not shown).

9  
10 Taking into account the above argumentation, we did not make changes in the revised manuscript.  
11



12  
13  
14 Figure rv.2.1. The bulge centre defined from the velocity (green dot) and as geometric mean position  
15 of the distribution of the tracer concentration field (yellow dot)  
16

17 **Comment 13.** On page 18, at line 20-22, why the bulge centre was closer to the coast in the case of  
18 the ideal bulge than in the case of the real bulge?

19 **Reply:** We rephrased this sentence, so that in now offers an explanation there.  
20

21 **Comment 14.** On page 30, what is the meaning of white blank area in the bulge in Figure 6 (left  
22 column)?

23 **Reply:** The blank area within the bulge is where the tracer concentrations were below the threshold  
24 values of the bulge definition. This is explained in the figure caption. We added (*see text for bulge*  
25 *definition*) in the figure caption of the revised ms.  
26

#### 27 Reference

- 28 Chao, S.-Y., 1990. Tidal modulation of estuarine plumes. *J. Phys. Oceanogr.* 20, 1115–1123.  
29 MacCready, P., Banas, N.S., Hickey, B.M., Dever, E.P., Liu, Y., 2009. A model study of tide- and  
30 wind-induced mixing in the Columbia River estuary and plume. *Cont. Shelf Res.* 29, 278–291.  
31 Zu, T., D. Wang, J. Gan, W. Guan, 2014. On the role of wind and tide in generating variability of  
32 Pearl River plume during summer in a coupled wide estuary and shelf system, *Journal of Marine*  
33 *System*, 136: 65-79.  
34 Maljutenko, I. and Raudsepp, U.: Validation of GETM model simulated long-term salinity fields in  
35 the pathway of saltwater transport in response to the Major Baltic Inflows in the Baltic Sea.  
36 IIEEE/OES Baltic International Symposium (BALTIC), 2014.

1 Nof, D., and Pichevin, T.: The Ballooning of Outflows. *J. Phys. Oceanogr*, 31(10), 3045-3058,  
2 2001.  
3 Pan, J., Gu, Y., and Wang, D.: Observations and numerical modeling of the Pearl River plume in  
4 summer season. *J. Geophys. Res.: Oceans*, 119(4), 2480-2500, 2014.  
5 Horner-Devine, A.R, Fong, D. A., Monismith, S. G. and Maxworthy, T.. Laboratory experiments  
6 simulating a coastal river inflow. *J. Fluid Mech.* 555, 203-232, 2006.  
7 Horner-Devine, A.R.: The bulge circulation in the Columbia River plume., *Cont. Shelf Res.*, 29,  
8 234-251, 2009.  
9  
10

# River bulge evolution and dynamics in a non-tidal sea – Daugava River plume in the Gulf of Riga, Baltic Sea

Soosaar, E., Maljutenko, I., Uiboupin, R., Skudra, M. and Raudsepp, U.

[1]{Marine Systems Institute at Tallinn University of Technology, Tallinn, Estonia}

Correspondence to: E.Soosaar (edith.soosaar@msi.ttu.ee)

## Abstract

Satellite remote sensing imagery and numerical modelling were used for the study of river bulge evolution and dynamics in a non-tidal sea, the Gulf of Riga (GoR) in the Baltic Sea. Total suspended matter (TSM) images showed a clearly formed anti-cyclonically rotating river bulge from Daugava River discharge during the studied low wind period. In about 7-8 days the bulge grew up to 20 km in diameter, before being diluted. ~~Bulge growth rate was estimated as  $r_b \sim t^{0.31 \pm 0.23}$  ( $R^2 = 0.87$ ).~~ A high resolution (horizontal grid step of 125 m) General Estuarine Transport Model (GETM) was used for detailed description of the development of the river plume in the southern GoR over the period when satellite images were acquired. In the model simulation, ~~bulge growth rate was estimated as  $r_b \sim t^{0.5 \pm 0.04}$  ( $R^2 = 0.90$ ).~~ Both the model simulation and the satellite images showed that river water was mainly contained in the bulge and there were numerous intrusions at the outer perimeter of the bulge. We made numerical sensitivity tests with actual bathymetry and measured river runoff without wind forcing: 1) having initial 3-dimensional density distribution; 2) using initially a homogeneous ambient density field. In the first case, the anti-cyclonic bulge did not develop within the course of the model simulation and coastal current was kept offshore due to ambient density-driven circulation. In the second case, the river plume developed steadily into an anti-cyclonically recirculating bulge, ~~with  $r_b \sim t^{0.28 \pm 0.01}$  ( $R^2 = 0.98$ ).~~ and a coastal current. ~~Additional simulations with constant cross-shore and along-shore winds~~ This showed a significant effect of the wind in the evolution of the river bulge, even if the wind speed was moderate ( $3-4 \text{ m s}^{-1}$ ). ~~In the second case,  $r_b \sim t^{0.28 \pm 0.01}$  ( $R^2 = 0.98$ ).~~ While previous studies conclude that mid-field bulge region is governed by balance between centrifugal, Coriolis and pressure gradient terms, our study showed that geostrophic balance is valid for the entire mid-field of the bulge, ~~except during the 1-1.5 rotation periods at the beginning of the bulge formation.~~ In addition, while there is discharge into the homogenous GoR in case of high inflow Rossby number, the river inflow might split into two jets, with strong mixing zone in-between, in the plume near field region.

## 1 **1 Introduction**

2 River water entering a coastal ocean typically forms a buoyant plume with an expanding anti-  
3 cyclonically rotating bulge near the river mouth and a coastal current in the coastally trapped wave  
4 direction (Fong & Geyer, 2002). Coastal currents are favoured in the case of low-discharge condi-  
5 tions and downwelling winds, while bulge formation is favoured during high-discharge conditions  
6 and upwelling winds (Chant et al., 2008). The anti-cyclonically recirculating bulge is characteristic  
7 of the surface advective plume (Yankovsky and Chapman, 1997) being a prominent feature in rotat-  
8 ing tank experiments and numerical simulations under ideal conditions (Avicola and Huq, 2003;  
9 Horner-Devine [et al.](#), 2006; Thomas and Linden 2007). Approximately 25-70% of river water is  
10 trapped in the bulge (Fong and Geyer, 2002).

11

12 Observational studies confirm that the bulge is a naturally occurring phenomenon with many rivers  
13 (Chant et al., 2008, Horner-Devine et al., 2008, Horner-Devine, 2009; Valente and da Silva, 2009;  
14 Saldias et al., 2012; Hopkins et al., 2013; Mendas et al., 2014; Pan et al., 2014; Fernández-Nóvoa et  
15 al., 2015), but an anti-cyclonic rotation inside a bulge is observed seldom (Kudela et al., 2010,  
16 Horner-Devine, 2009; Chant et al., 2008). Observations of the evolution of the bulge over a certain  
17 time period are almost non-existent, with the exception of the Niagara River plume (Horner-Devine  
18 et al., 2008) and the Tagus estuary plume (Valente and da Silva, 2009). However, both cases are  
19 without clear evidence of anti-cyclonic circulation within the bulge.

20

21 In natural conditions, the evolution of the bulge is affected by properties of the outflow (Yankovsky  
22 and Chapman 1997; Avicola and Huq 2003a), tides (Valente and da Silva, 2009), wind (Dzwon-  
23 kowski and Yan, 2005; Whitney and Garvine 2005) and the ambient coastal current (Fong and  
24 Geyer 2002). Thus, the evolution of the structure and circulation inside the bulge is difficult to ob-  
25 serve. Exploitation of optical satellite remote sensing has extended the possibilities of monitoring  
26 and understanding the river plume dynamics under various hydrological, morphological and hydro-  
27 dynamical conditions. A number of existing papers provide composite maps, where plume location  
28 and structure is described in response to prevailing wind conditions. Neither evolution of the bulge  
29 nor anti-cyclonic circulation within it can be identified from the composite satellite remote sensing  
30 images. Although each river plume can be considered as specific, Horner-Devine et al. (2015) have  
31 summarized the dynamics of an anti-cyclonically rotating bulge, with special emphasis on the river  
32 water volume re-circulating within the bulge. In their study, with reference to Nof and Pichevin  
33 (2001), they summarize that with stronger anti-cyclonic circulation within the bulge, more water  
34 recirculates in the bulge.

1

2 The aim of the present paper is to provide additional evidence of a well-developed anti-cyclonically  
3 rotating river bulge, using consecutive optical remote sensing images from a non-tidal sea and to  
4 assess current theoretical understanding of river bulge internal structure and dynamics from the  
5 complementary numerical model simulation results. We focus on the evolution of an anti-  
6 cyclonically rotating bulge during one life-cycle, i.e. from its formation until its dilution with ambi-  
7 ent water. The horizontal expansion of the bulge from remote sensing imagery and the reproduction  
8 by numerical simulation are compared with modelled undisturbed bulge development and existing  
9 theoretical knowledge. The bulge depth, volume of the river water trapped in the bulge and the  
10 movement of the bulge centre are evaluated from model experiments. The validity of gradient wind  
11 (or cyclostrophic) balance (see equation (2) below) is evaluated for specific time instants in the  
12 mid-field region of the plume.

13

14 The eastern sub-basin of the Baltic Sea, the Gulf of Riga (GoR), is used as the study area (Fig. 1a).  
15 The GoR is almost bowl-shaped, has brackish water and is semi-enclosed (connection with the Bal-  
16 tic Sea through the Irbe Strait, 25 m deep, minimum cross-section area 0.4 km<sup>2</sup> and through the  
17 Virtsu Strait which is 5 m deep, minimum cross-section area 0.04 km<sup>2</sup>). [The circulation in the GoR](#)  
18 [is mainly driven by wind forcing and 3-dimensional density gradient forcing \(Raudsepp et al. 2003,](#)  
19 [Soosaar et al., 2014, Lips et al. 2016\). The mean circulation in spring consists of two main gyres,](#)  
20 [with the cyclonic gyre covering the eastern and the anti-cyclonic gyre covering the western part of](#)  
21 [the GoR \(Soosaar et al. 2014 Fig. 2.\). This two-gyre system, which may transform into a single](#)  
22 [anti-cyclonic gyre/cyclonic gyre covering most of the basin area during the warm/cold season](#)  
23 [\(Lips., et al., 2016\).](#) Small tidal oscillation (O [0.01-0.1 m]; Keruss and Sennikovs, 1999) allows us  
24 to consider it as a non-tidal estuary. The main freshwater source for the GoR is Daugava River in  
25 the south-east with a high discharge of 2500 m<sup>3</sup> s<sup>-1</sup> in early spring, which decreases to 200 m<sup>3</sup> s<sup>-1</sup> in  
26 late summer. The present study concentrates on the period from the last 12 days of March and early  
27 April 2007, when there was a high discharge of ~2500 m<sup>3</sup> s<sup>-1</sup> and low wind.

28

## 29 **2 Materials and methods**

### 30 **2.1 Satellite Data**

31 [ENVISAT/MERIS \(Medium Resolution Imaging Spectrometer\) data with a 300m resolution from](#)  
32 [the CoastColour database \(http://www.coastcolour.org/data/archive/\) was used for monitoring bulge](#)  
33 [dynamics and structure. MERIS was designed to monitor coastal waters \(Doerffer et al. 1999\), and](#)

1 ~~it~~ therefore, it has sufficient spectral resolution in the range of wavelengths above 555 nm for moni-  
2 ~~toring-of~~ turbid and optically complex waters like the Baltic Sea (Gitelson et al. 2009). MERIS im-  
3 ~~agery was preferred to other similar sensors (e.g MODIS) as (i) MERIS based water quality retriev-~~  
4 ~~als in optically complex case-2 waters of the Baltic Sea are more accurate due to better performance~~  
5 ~~of the atmospheric correction algorithm (Goyens et al. 2013). In addition, -and (ii) MERIS has~~  
6 ~~higher spatial resolution (300m), which enables to resolve detailed features of the river bulge. The~~  
7 ~~MERIS images were processed using the Case-2 Regional (C2R) algorithm (Doerffer and Schiller~~  
8 ~~2007, Doerffer and Schiller 2008) in the BEAM software package ([http://www.coastcolour.org/data/archive/](http://www.brockmann-</a></del><br/>9 <del>consult.de/cms/web/beam/) in order to apply atmospheric correction and to obtain the reflectance</del><br/>10 <del>values used for TSM retrieval. The following pixel quality flags/masks provided in the Level1</del><br/>11 <del>Coast Colour product and in the Level 2 C2R product were used to mask the invalid pixels affected</del><br/>12 <del>by the following phenomena: land, whitecaps, sun glint, cloud, cloud shadow, snow and ice. The</del><br/>13 <del>C2R algorithm has been validated in various locations in the optically complex waters of the Baltic</del><br/>14 <del>Sea and it has proven to be suitable for water quality monitoring (e.g. Siitam et al 2014, Attila et al.</del><br/>15 <del>2013, Vaičiūtė et al 2012). We used total suspended matter (TSM) concentrations as a marker to</del><br/>16 <del>distinguish turbid river water from “clear sea water”;</del> as TSM shows stronger contrast compared to<br/>17 <del>other biological and physical parameters (SST, CHL etc). Moreover, Also a comparative study by</del><br/>18 <del>Beltrán-Abaunza et al. (2014) showed that TSM concentrations are more accurately retrieved by</del><br/>19 <del>different standard remote sensing algorithms (including C2R) than-the other water constituents. An</del><br/>20 <del>overall of seven sufficiently cloud free images were available from 20, 26, 27, 29, 30 March and 1</del><br/>21 <del>and 4 April. The images were acquired at about 9 a.m.UTC. The satellite data was interpolated to a</del><br/>22 <del>regular 0.3km 0.3 km grid on the UTM-34v projection. Then the TSM concentrations were</del><br/>23 <del>smoothed using a 3 3 point median filter.</del><br/>24 <del>ENVISAT/MERIS (Medium Resolution Imaging Spectrometer) data with 300 m resolution (from</del><br/>25 <del><a href=)) was used for monitoring bulge dynamics and structure.~~  
26 ~~The MERIS images were processed using the Case 2 Regional algorithm (Doerffer and Schiller,~~  
27 ~~2007). We used total suspended matter (TSM) concentrations as a marker to distinguish turbid river~~  
28 ~~water from “clear sea water”, as TSM shows stronger contrast compared to other biological and~~  
29 ~~physical parameters (SST, CHL etc). In studies performed by Siitam et al. (2014) and Attila et al.~~  
30 ~~(2013), the reliability of the algorithm for TSM estimation in the coastal Baltic Sea was confirmed.~~  
31 ~~An overall of seven sufficiently cloud free images were available from March 20th, 26th, 27th,~~  
32 ~~29th, 30th and April 1st and 4th. The images were acquired at about 9 a.m, UTC. The satellite data~~  
33 ~~was interpolated to a regular 0.3x0.3 km grid on the UTM 34v projection. Then the TSM concentra-~~  
34 ~~tions were smoothed using a 3x3 point median filter.~~

## 2.2 River runoff and wind data

Daily volume flux for Daugava River was measured 35 km upstream from the river mouth (coordinates – 56.8516 N; 24.2728 E). Daily volume flux for Gauja and Lielupe rivers (*see* Fig. 1 for locations) was calculated from measured data. As locations of measurement stations are 55 km and 95 km from the river mouth, the measured data was multiplied by factors 1.05 and 1.87 respectively<sup>1</sup>, in order to obtain river discharge at the river mouth. The coefficients are obtained as a ratio between the whole catchment area of those rivers and the catchment area of those rivers up until the stations where the river flow was measured.

Wind data at one hour intervals was obtained from Ruhnu weather station, which is located on the Ruhnu Island in the central area of the Gulf of Riga (Fig. 1 and 2).

## 2.3 Numerical model setup: GETM

For numerical simulation we used the fully baroclinic and hydrostatic ocean model GETM (General Estuarine Transport Model (Burchard and Bolding, 2002)) that is coupled to the GOTM (General Ocean Turbulence Model (Umlauf and Burchard, 2005)) for vertical turbulence parameterization. The GETM uses a spherical coordinate system in the horizontal plane and a bottom-following vertical coordinate system. Using a mode splitting technique, GETM solves water dynamics on the Arakawa C-grid (Arakawa and Lamb, 1977). The GETM is characterized by advanced numerical techniques of advection schemes and internal pressure discretization schemes that minimize computational errors (Stips et al., 2004; Burchard and Rennau, 2008). In our setup we used the total variance diminishing (TVD) advection scheme for salinity, temperature and momentum (Pietrzak, 1998) and internal pressure parameterization suggested by Shchepetkin and McWilliams (2003). In our setup we used the third-order monotone total variance diminishing (TVD) advection scheme with the P2-PDM limiter and a half step directional split approach for salinity, temperature and momentum. Advection scheme TVD-P2-PDM was selected, as it has shown lower discrete variance decay rates than other widely used advection schemes (Pietrzak 1998, Klingbeil 2014). Temporal discretization was conducted with a coupled explicit mode splitting technique for barotropic and baroclinic modes.

---

<sup>1</sup>Methodology worked out and in use for Gauja and Lielupe rivers in LVGMC - Latvian Environment, Geology and Meteorology Centre Institute. <http://www.meteo.lv/en/>.

1 The model domain covered the GoR with closed boundaries at the Irbe Strait and the Virtsu Strait.  
2 In the study by Soosaar et al. (2014), comparison of monthly mean circulations, with the Irbe and  
3 Suur straits being either closed or opened, showed only minor differences that occur mostly near the  
4 straits. The coefficient of determination between the two cases for April 1998 was  $R^2=0.93$ . Our  
5 analyses of model simulations concentrate on the south-eastern part of the GoR, where the effect of  
6 closed straits is expected to be negligible over the simulation time period of two weeks. Topography  
7 was prepared using The Baltic Sea Bathymetry Database (BSHC 2013) and interpolated to a 125 m  
8 regular grid. Depths at the head of Daugava were adjusted to include Riga harbour fairway (depth 7  
9 m). The vertical water column was split into 30 density adaptive layers, giving a vertical resolution  
10 of under 0.5 m within the stratified bulge area (Gräwe et al. 2015). The barotropic time step was  
11 three seconds and the baroclinic time step 60 seconds. Hourly river run-off input from the meas-  
12 urements of three rivers, Daugava, Lielupe and Gauja, were included. Daugava run-off was equally  
13 distributed over 7 grid cells. Three rivers, Daugava, Lielupe and Gauja, were included. The mete-  
14 orology was adopted from the EMCWF ERA-Interim dataset with a lateral resolution of  $1/4^\circ$  and a  
15 temporal resolution of 6 h (Dec et al., 2011). ~~The meteorology was adopted from EMCWF ERA-~~  
16 ~~Interim dataset (Dec et al., 2011)~~

Formatted: Superscript

17  
18  
19 The model simulation covered the period from 20 March to 5 April 2007. Initial salinity fields were  
20 interpolated from the 1 nautical mile simulation for the Baltic Sea (Maljutenko and Raudsepp  
21 2014). The density only depended on salinity. A 3-day spin-up period with a realistic salinity field  
22 and a linear increase of river run-off from zero to the measured river run-off value on 20 March  
23 2007 was used before including wind forcing on 20 March (real simulation). TSM was used as a  
24 passive tracer for the detection of river water spreading in the model simulation. Initial TSM con-  
25 centration was set to with-zero initial concentration in the GoR and the TSM concentration in river  
26 water was set to a unit value. The passive tracer was released to the GoR only as the Daugava River  
27 load of TSM, being proportional to the Daugava River run-off starting from 20 March. and with  
28 unit concentration load from rivers was set as tracer variable.

Formatted: Font color: Black, English (United Kingdom)

## 30 2.4 Model validation

31 In situ measurements suitable for the model validation from the study area during high Daugava  
32 River runoff are ferry-box measurements on -board the ship travelling between Riga and Stock-  
33 holm. The available measurements for the estimation of the-model ability of the model to reproduce  
34 Daugava River bulge dynamics cover the period from 20 March to 4 April 2014. This period com-

prises the increase of the Daugava River runoff from  $600 \text{ m}^3 \text{ s}^{-1}$  ~~to until~~ the peak value of  $1100 \text{ m}^3 \text{ s}^{-1}$  and the decrease of the runoff to  $800 \text{ m}^3 \text{ s}^{-1}$  (Fig. 3a). In total, eight transects from the Daugava River mouth to the central GoR with 2-day intervals fall into the period (Fig. 1). The model setup for the validation run was made similarly to the one described in Sec. 2.3. ~~The d~~Daily river run-off input from the measurements of the Daugava River was included. The meteorology was adopted from the HIRLAM-ETA dataset, with a lateral resolution of 11 km and a temporal resolution of 3 h (Unden et al., 2002). Initial salinity fields were interpolated from the HIROMB 1 nautical mile simulation for the Baltic Sea on 20 March 2014 (Funkquist and Kleine, 2000). The density only depended on salinity. No spin-up period was included.

The ~~m~~Mid-field bulge front can be characterized ~~as by~~ the location of maximum salinity gradient. We calculated the salinity gradient along the ship transect from measurements and model results. Maximum gradient location from in situ measurements stayed mostly at 5 km from the river mouth (Fig. 3c). There are two exceptions, on 29 March and 2 April, when the maximum gradient was located at 10 km (Fig. 3c) following a period of wind to the west (Fig. 3b). In the model simulation, the bulge front ~~increases-d~~ from 1 km on 21 March to 15 km on 24 March. That period corresponds to the period of increase of river runoff and low winds (Fig. 3a,b). Since the evening of 24 March the wind speed increased and the bulge was destroyed. The front ~~retreated to a position was back~~ at 1 km from the river mouth. The ~~b~~Bulge started to increase on 27 March and reached a maximum extent of 20 km on ~~theat~~ night of 28 March. This corresponds to a peak in river runoff and calm winds. During the rest of the simulation period, the bulge front remained between 2 and 10 km. The root mean square deviation between the locations of simulated and observed bulge front was 2.4 km.

### 3 Results

#### 3.1 Satellite imagery and model simulation

The first satellite image on 20 March showed the development of three river plumes. The Daugava River plume was far larger (about 8 km in diameter) than Gauja and Lielupe river plumes (Fig. 34a) ~~which can also be seen on the numerical model (Fig. 4h)~~. The wind conditions favoured the development of river plumes. From 15 to 19 March, wind speed increased from 2 to  $10 \text{ m s}^{-1}$  (Fig. 2b), which could have generated sufficient mixing to destroy previously formed river plumes as well as avoided the development of a clearly distinguishable river plume. Just prior to the first satellite image, the wind speed dropped from  $11 \text{ m s}^{-1}$  to  $2 \text{ m s}^{-1}$ , which may have considerably reduced wind

1 mixing and enabled the free development of river plumes. From 17 to 20 March Daugava River  
2 discharge increased from  $1500 \text{ m}^3 \text{ s}^{-1}$  to  $2500 \text{ m}^3 \text{ s}^{-1}$  (Fig. 2a). The discharges of Lielupe and Gauja  
3 rivers were  $230 \text{ m}^3 \text{ s}^{-1}$  and  $180 \text{ m}^3 \text{ s}^{-1}$  respectively. The river plumes were well distinguishable, as  
4 the ambient TSM concentrations was  $2 \text{ g m}^{-3}$ , compared to  $20 \text{ g m}^{-3}$  in the bulge centre, in the  
5 southern part of the GoR (Fig. 4a). In all three cases, the river water had most likely initially spread  
6 offshore, then turned to the right and formed a coastal current. In the bulge, current velocities were  
7 up to  $50 \text{ cm s}^{-1}$ , while ambient currents were about  $5 \text{ cm s}^{-1}$  (Fig. 4h). ~~Thus, a~~All three plumes con-  
8 sisted of a bulge area and a coastal current (Fig. 4a). Coastal current was detached from the coast,  
9 leaving a stripe of lower TSM water near the coast (Fig. 4a,h). The offshore location of the maxi-  
10 imum currents parallel to the coast and a counter-current at the coast (Fig 4h) were remnants of the  
11 previous spreading of river water together along with wind- and density-driven currents in the GoR.  
12 Lielupe River plume was less pronounced than other river plumes, due to the blocking effect of the  
13 Daugava River plume on the right and the decline of the river discharge.

14  
15 ~~The wind conditions favoured the development of river plumes. From 15 to 19 March, wind speed~~  
16 ~~increased from  $2$  to  $10 \text{ m s}^{-1}$  (Fig. 2b), which could have generated sufficient mixing to destroy pre-~~  
17 ~~viously formed river plumes as well as avoided the development of a clearly distinguishable river~~  
18 ~~plume. Just prior to the first satellite image, the wind speed dropped from  $11 \text{ m s}^{-1}$  to  $2 \text{ m s}^{-1}$ , which~~  
19 ~~may have considerably reduced wind mixing and enabled the free development of river plumes.~~

20  
21 The next image was obtained on 26 March. Checking the sequence of tracer spreading in the nu-  
22 merical model showed that the plume on 26 March was the result of the reset of the river plume on  
23 24 March. The winds of  $6 \text{ m s}^{-1}$  from the northeast had hampered the free development of the river  
24 plume by mixing river water and transporting it offshore. The Daugava River bulge had a diameter  
25 of grown significantly, to  $\sim 16 \text{ km}$  in diameter (Fig. 4b). The core of the bulge was almost circular,  
26 with many intrusions along the outer rim. In the core of the bulge, freshly discharged water with  
27 high TSM concentration formed a jet with an anti-cyclonic spreading pattern along the left side of  
28 the bulge. The existence of coastal current could not be verified on the satellite image and the bulge  
29 manifested itself as more of a separate feature of the plume. The coastal current had formed as a  
30 narrow band pressed against the coast in the numerical model (Fig. 4i). Since the reset of the river  
31 plume on 24 March, Meanwhile the wind had been from the northeast, with the speed dropping  
32 from  $6$  to  $2-6 \text{ m s}^{-1}$  (Fig. 2b, c). As shown in Sec. 3.2, This type of upwelling favourable wind  
33 may push the bulge offshore and may cause several intrusions at the open sea area of the bulge (Fig  
34 6b). Model simulation showed strong background anti-cyclonic circulation of about  $20 \text{ cm s}^{-1}$  in the

1 ~~south-eastern GoR (Fig. 4i). have caused slight upwelling at the southeastern coast, downwind~~  
2 ~~coastal currents over the shallow area and an offshore Ekman drift, resulting in the destruction of~~  
3 ~~the coastal current and separation of the bulge.~~ The Gauja River plume consisted of a bulge area and  
4 a coastal current attached to the coast. ~~In the previous image, the coastal current of Gauja River~~  
5 ~~plume had been slightly detached from the coast.~~ The Lielupe River plume was almost undetect-  
6 able, as the volume discharge had decreased to  $130 \text{ m}^3 \text{ s}^{-1}$ .

7  
8 During the next 4 days, i.e. until 30 March, the wind speed was very low, between  $0\text{--}23 \text{ m s}^{-1}$ . We  
9 may assume that wind-driven currents and mixing were negligible. The Daugava River bulge re-  
10 mained almost circular and further detached from the coast (Fig. 4c-e, i-l). The main feature within  
11 the bulge was anti-cyclonically turning river water with high TSM concentration (Fig. 34c-e) and  
12 well-established anti-cyclonic circulation in the bulge, with a characteristic current speed of  $20 \text{ cm}$   
13  $\text{s}^{-1}$  (Fig. 4i-l). This gives direct confirmation that water in natural buoyant bulges circulates anti-  
14 cyclonically in the northern hemisphere. More water intruded the southern GoR at the western  
15 boundary of the bulge. Even low onshore wind may cause significant intrusions at the western  
16 boundary of the bulge (Fig 6d). This intrusion spread anti-cyclonically, probably due to ambient  
17 circulation, and diluted with surrounding water. No clear coastal currents were visible.

18  
19 By 1 April, the wind speed had increased to  $4 \text{ m s}^{-1}$  and was blowing from the north. Daugava River  
20 discharge had reduced from  $\sim 2000$  to  $\sim 1500 \text{ m}^3 \text{ s}^{-1}$  (Fig. 2). The image from 1 April still showed a  
21 circular bulge with a notably smaller TSM concentration than previously (Fig. 34f). The bulge had  
22 been transported westward and was nearly detached from the Daugava River outlet. The numerical  
23 model captured the tendency of westward transport of the bulge from 30 March to 1 April, but the  
24 bulge was more distorted (Fig. 4 m). The strong wind event of  $10 \text{ m s}^{-1}$  on 2 April had destroyed the  
25 bulge and river water with higher TSM concentration had smeared over the southern GoR by 4  
26 April (Fig. 34g,n).

### 27 **3.2 Realistic simulation**

28 ~~The numerical model provides an opportunity for better and more detailed description of the devel-~~  
29 ~~opment of the river plume in the southern GoR over the period when satellite images were acquired.~~  
30 ~~The model considers TSM input only from the river discharges (no biology or resuspension from~~  
31 ~~the sediments).~~

1 ~~Daugava bulge had developed by 20 March in the numerical model (Fig. 3h). In the bulge, current~~  
2 ~~velocities were up to  $50 \text{ cm s}^{-1}$  while ambient currents were about  $5 \text{ cm s}^{-1}$ . Strong momentum input~~  
3 ~~by rivers caused spreading of tracers away from the coast, which matched the SPM pattern on the~~  
4 ~~satellite image. In the case of the Daugava River plume, coastal counter current blocked the spread-~~  
5 ~~ing of tracers at the coast and the formation of a classical coastal current of the river plume. The~~  
6 ~~offshore location of the maximum currents parallel to the coast and counter current at the coast~~  
7 ~~were remnants of the previous spreading of river water together with wind and density driven cur-~~  
8 ~~rents in the GoR.~~

9  
10 By 26 March, bulge has not expanded as much as would be expected (Fig. 3i) based on satellite  
11 images from 20 and 26 March (Fig. 3a, b). In addition to strong momentum input from Daugava  
12 River, where current velocities were up to  $30 \text{ cm s}^{-1}$  in the bulge, the strong background anti-  
13 cyclonic circulation of about  $20 \text{ cm s}^{-1}$  prevailed over the south eastern GoR. This circulation had  
14 pushed previous river water offshore and supported northward intrusion of bulge water. ~~The coastal~~  
15 ~~current had formed as a narrow band pressed against the coast. Bulge orientation, offshore extent,~~  
16 ~~northward intrusion at the northern rim and south westward intrusion at the south western rim of~~  
17 ~~the bulge were qualitatively comparable to similar features on the satellite image. Checking the se-~~  
18 ~~quence of tracer spreading in the numerical model showed that the plume on 26 March was the re-~~  
19 ~~sult of the reset of river plume on 24 March. The winds of  $6 \text{ m s}^{-1}$  from the northeast had hampered~~  
20 ~~the free development of the river plume by mixing river water and transporting it offshore. Further~~  
21 ~~developments of the Daugava River plume and especially the bulge until 30 March were quite con-~~  
22 ~~sistent in the model and on the satellite images (Fig. 3i 1). Well established anti cyclonic circulation~~  
23 ~~in the bulge, with a characteristic current speed of  $20 \text{ cm s}^{-1}$ , was confirmed in the model results.~~  
24 ~~The numerical model captured the tendency of westward transport of the bulge from 30 March to 1~~  
25 ~~April. The bulge retained a circular shape on the satellite image, but was more distorted in the~~  
26 ~~model (Fig. 3l, m). The numerical model showed that the regular river plume started to distort on 31~~  
27 ~~March (Fig. 3n). The strong wind event of  $6-10 \text{ m s}^{-1}$  on 2 April started to destroy the bulge in the~~  
28 ~~model as well (Fig. 2).~~

### 30 **3.23 Idealized simulations**

31 In the realistic model simulation, the Daugava River plume was affected by river discharge, ambient  
32 currents and wind-driven currents. We made numerical sensitivity tests with 1) river discharge into  
33 a stratified GoR, while wind forcing was switched off; 2) river discharge into a homogeneous GoR

1 with an ambient water salinity of  $6 \text{ g kg}^{-1}$ , while wind forcing was switched off (ideal simulation).  
2 In the first case, the anti-cyclonic bulge did not develop within the course of the model simulation  
3 and the coastal current was kept offshore due to ambient circulation (Fig. 45a). In the ideal run,  
4 river plume developed steadily into an anti-cyclonically recirculating bulge and a coastal current  
5 (Fig. 45b). The bulge length (offshore extent) and width (along-shore extent) as well as the width of  
6 the coastal current increased steadily in the course of the model simulation.

7  
8 Additional simulations with cross-shore and along-shore winds were made with wind speeds of 2  
9 and  $4 \text{ m s}^{-1}$ . A wind speed of  $2 \text{ m s}^{-1}$  caused minor, if any, alterations if any in the case of all wind  
10 directions (not shown). A wind speed  $4 \text{ m s}^{-1}$  altered the bulge in agreement with the classical  
11 Ekman transport theory. The alongshore downwelling favourable wind pushed the bulge towards  
12 the coast and the coastal current was well-developed (Fig. 6a). The alongshore upwelling favour-  
13 able wind pushed the bulge offshore, so that the bulge was detached from the coast and no coastal  
14 current developed (Fig 6b). The bulge had irregular shape with several intrusions at the open sea  
15 area of the bulge. In case of offshore wind, the bulge mid-field region was less uniform, was  
16 more flat and coastal current was enhanced (Fig. 6c). Onshore wind tilted the bulge to the up-  
17 coast direction, with significant intrusions at the upcoast rim of the bulge (Fig. 6d). Coastal current  
18 was restrained and had an irregular shape. Thus, comparison of the real run with test cases  
19 showed a significant effect of wind in the evolution of the river bulge, even if wind speed was mod-  
20 erate (*see* Fig. 2b).

### 22 **3.34 Temporal evolution of the bulge**

23 The evolution of the river bulge is classically described by the spreading of the offshore front of the  
24 bulge and an increase of bulge depth (e.g. Avicola and Huq 2003, Horner-Devine *et al.* 2006). There  
25 are uncertainties in the determination of the edges of a bulge as well as the volume of a bulge. In  
26 natural conditions, diffusion and mixing at the edges dilutes river water with surrounding water  
27 (Horner-Devine *et al.* 2015). Multiple previous studies defined the bulge edge based on a pre-  
28 lected threshold value. Horner-Devine *et al.* (2006) choose a constant 20% buoyancy contour as the  
29 reference value. Gregorio *et al.* (2011) used a reference velocity,  $1.7 \text{ cm/s}$ , to define the coastal cur-  
30 rent front. Soosaar *et al.* (2015) defined the bulge edge to be 10% from the discharge depth.

31  
32 We used TSM concentration to define the bulge boundary. On the satellite images, the threshold  
33 values were selected after a visual inspection of TSM concentration maps. Horner-Devine *et al.*

~~(2008) have used a threshold value of normalized water leaving radiance (nLw) in the 555 nm band to define the edges of the Niagara River plume on SeaWiFS satellite images. Our main criterion was to capture the circular part of the bulge and neglect coastal current as well as most of the intrusions. The threshold concentration varied from image to image as: 1) the TSM concentration of river water was variable and unknown for us; 2) locally, TSM concentration may have changed due to biological activity. The threshold value of  $\log_{10}(TSM)$  was 1.0 for the image on 20 March, 1.2 for the images on 26, 27, 29 and 30 March and 1.1 for the image on 1 April. No bulge was defined for the image on 4 April. We checked the option to define the edges of the bulge, using spatial gradients of the TSM concentrations. Firstly, this approach did not eliminate the uncertainties, as the local maximum gradient isolines were discontinuous. Secondly, the boundaries of the bulge did not differ significantly from the boundaries that were determined using a threshold value for TSM concentration. In the numerical model, the bulge boundary was defined where  $I = \log_{10}(TSM) > -0.15$ . Different values of  $I > -0.05, -0.10, -0.20, -0.25$  were also used for the bulge boundary. The bulge radius increases with decreasing  $I$  (Fig. 7b) as well as bulge mean depth (not shown), but the dynamics of the bulge does not depend on the selected threshold value for the bulge boundary.~~

Formatted: Font: Italic

We compared the temporal evolution of mean depth, radius and volume of the real and the ideal bulge from the numerical model.

~~In order to be consistent with previous river bulge studies (Horner-Devine, 2009; Horner-Devine et al., 2008; Horner-Devine et al., 2006), the bulge effective radius,  $r_b$ , was estimated through the area of the bulge,  $A_b$ , assuming a circular shape of the bulge~~

$$r_b = \left( \frac{A_b}{\pi} \right)^{\frac{1}{2}}. \quad (1)$$

According to the criterion of the bulge definition, the bulge is defined after about  $0.5T$ , where  $T$  is rotation period of the earth (Fig. 57a, b) and  $T=0 \equiv 24$  March 2007 05:00. Steady increase of the real bulge took place during seven rotation periods. Both mean depth and radius as well as the volume were larger for the real bulge than for the ideal bulge. We would like to note the pulsation of the actual-real bulge - when bulge diameter increased, bulge mean depth decreased and vice versa. The decrease of the bulge diameter was faster than the decrease of bulge mean depth during the dissipation phase, which started from  $7T$ . Occasionally, bulge depth even increased. Thus, the water in the bulge was mixed deeper during the dissipation phase.

1  
2 The volume of river water that went into the bulge increased relatively fast during the first two rota-  
3 tion periods (Fig. 57c). In the real case, almost 60% of river water was trapped inside the bulge,  
4 while in the ideal case the volume reached 45%. We estimated the volume that was transported  
5 away by the coastal current. In order to be consistent with our bulge definition, we calculated water  
6 flow at the transect through the model grid cells where  $I > -0.15$ . During 2T, a negligible amount of  
7 river water was transported by the coastal current. During 2T the fraction of river water inside the  
8 bulge decreased monotonically, while the volume of coastal current increased (not shown). In the  
9 real case, water volume in the bulge increased until the bulge started to dissipate, but steadily re-  
10 tained its 50 % river water content. The fraction of river water started to increase from 4T, but did  
11 not exceed 5% until the end of the simulation. In the case of the real bulge, our estimations showed  
12 that about 50% of river water could be determined as either coastal current or as bulge due to intru-  
13 sions and mixing at the boundaries of the bulge and the coastal current (see Fig. 34), unless we  
14 broaden the definition of the bulge. Still, it is obvious from satellite images and simulation results  
15 that a far larger amount of river water stayed within the bulge and was transported offshore by in-  
16 trusions than the amount that formed a coastal current. In the ideal bulge, the fraction of river water  
17 decreased after 2T, while the coastal current increased. During 11T, the fraction of volume in the  
18 bulge and in the coastal current equilibrated. Thus, we may conclude that in the present case of the  
19 Daugava River plume, density- and wind-driven currents oppose the development of the coastal  
20 current.

21  
22 The bulge radius was non-dimensionalized with the bulge Rossby radius

$$L_b = \left( \frac{2Qg'}{f^3} \right)^{\frac{1}{4}} \quad (2)$$

25  
26 where  $Q$  is river runoff. In our case, the bulge Rossby radius varied between 2.7 and 3.1 km in time,  
27 according to the actual runoff of the Daugava River. Time series of increase of non-dimensional  
28 bulge radius from numerical simulations are presented in Fig. 7d. We approximated the growth rate  
29 of the bulge radius using a power function. In the real case, we excluded the time period when the  
30 bulge started to dissipate, i.e. ~~keeping maintaining~~ the values ~~until~~ up to 8T. The real and the ideal  
31 simulations gave  $r_b \sim t^{0.50 \pm 0.04}$  and  $r_b \sim t^{0.28 \pm 0.01}$ , with the coefficients of determination being  $R^2 = 0.90$   
32 and  $R^2 = 0.98$ , respectively. Thus, in the real model simulation, the growth of the bulge radius was  
33 faster than in the ideal simulation. It can be explained by prevailing upwelling favourable winds

Field Code Changed

(Fig. 2b,c)- which even with a speed of 3-4 m s<sup>-1</sup> restrained the development of a coastal current and retained more water remains in the bulge (Fig. 6b). Using the thermal wind balance, Avicola and Huq (2003) estimated the growth rate of the bulge radius  $r_b \sim t^{1/4}$ , although in the laboratory experiments they obtained the growth rate  $r_b \sim t^{2/5}$ . From laboratory experiments, Horner-Devine et al. (2006) estimated that a buoyant surface advective bulge expands radially as  $\sim t^{1/4}$  during the first 5 rotation periods and later as  $\sim t^{2/5}$  at later times. The measurement study for the Niagara River bulge (Horner-Devine et al., 2008) gave  $\sim t^{0.46 \pm 0.29}$ .

### 3.45 Bulge momentum balance

The dynamics of the river bulge are described as balance between centrifugal, Coriolis and pressure gradient terms:

$$\frac{v_\theta^2}{r} + fv_\theta = g' \frac{\partial h}{\partial r} \quad (23)$$

as hypothesized by Yankovsky & Chapman (1997) and confirmed by Horner-Devine (2009) for the Columbia River plume. In (23), the  $v_\theta$  is depth averaged angular velocity,  $r$  is radial distance from the bulge centre,  $f$  is Coriolis' parameter,  $g'$  is reduced gravity and  $h$  is bulge thickness. Left side of the equations is centrifugal (T1) and Coriolis term (T2) respectively, right side of the equation is pressure gradient term (T3). We calculated these terms for the case of the real bulge and the ideal bulge development on 29 March 2007 at 20:00 (Fig. 68). As was the case previously, the bulge was defined where  $I > -0.15$ . The currents were strongest at the steepest slope of the bulge (Fig. 68a, b). Although the ideal and real bulges were similar quantitatively, the bulge centre was much closer to the coast (3 km) for the ideal bulge than for the real bulge (6 km). The outer thin area of the ideal bulge was wider than in the case of the real bulge. All terms in (23) showed higher absolute values at the steepest slope of the bulge (Fig. 68c-h). With the exception of the near field region, the centrifugal force was nearly an order of magnitude smaller than the Coriolis' term and the pressure gradient term. Geostrophic balance was valid for the entire mid-field of the bulge (Fig. 68m, n). Taking into account the balance, (23), the error even increased slightly (Fig. 68o, p).

We calculated the time series of spatially averaged momentum balance terms, Eq. (3), for the ideal (Fig. 9a) and the real bulge (Fig. 9b). In the case of the ideal bulge, all three terms contributed sig-

Comment [O1]: aeg kogu lõigus

nificantly to the momentum balance during the initial phase of bulge development, i.e. up until 1T (Fig. 9a). Between 1T and 2T the contribution from the centrifugal force decreased, so that this term became nearly an order of magnitude smaller than the Coriolis term and the pressure gradient term. In the case of the real bulge, the centrifugal force component also decreased during 1T and 2T (Fig. 9b). However, already at the beginning, the initial value of the centrifugal force was an order of magnitude smaller than the Coriolis and pressure terms from the beginning. The Coriolis and pressure gradient terms does not have clear increasing or decreasing trend.

### 3.6 Non-dimensional bulge spreading

The bulge radius was non-dimensionalized with the bulge Rossby radius

$$L_b = \left( \frac{2Qg'}{f^3} \right)^{\frac{1}{4}} \quad (3)$$

where  $Q$  is river runoff. In our case, the bulge Rossby radius varied between 2.7 and 3.1 km in time, according to the actual runoff of the Daugava River. Time series of increase of non-dimensional bulge radius from satellite images and the respective numerical simulations are presented in Fig. 7. We approximated the growth rate of the bulge radius using a power function. In the real case, we excluded the time period when the bulge started to dissipate, i.e. keeping the values until 8T. The satellite remote sensing and the ideal simulation gave  $r_b \sim t^{0.31 \pm 0.23}$  and  $r_b \sim t^{0.28 \pm 0.01}$ , with the coefficient of determination being  $R^2 = 0.87$  and  $R^2 = 0.98$ , respectively. In the real simulation,  $r_b \sim t^{0.50 \pm 0.04}$  ( $R^2 = 0.90$ ). Thus, in the real model simulation, the growth of bulge radius was faster than in the ideal simulation. Using the thermal wind balance, Avicola and Huq (2003) estimated the growth rate of the bulge radius  $r_b \sim t^{1/4}$ , although in the laboratory experiments they obtained the growth rate  $r_b \sim t^{2/5}$ . From laboratory experiments, Horner Devine et al. (2006) estimated that a buoyant surface advective bulge expands radially as  $t^{1/4}$  during the first 5 rotation periods and as  $t^{2/5}$  at later times. The measurement study for the Niagara River bulge (Horner Devine et al., 2008) gave  $t^{0.46 \pm 0.29}$ .

## 4 Discussion

A prominent feature in the satellite images and the model simulations was a well-developed anti-cyclonic circulation in the river bulge, which persisted for about 7-8 days. High river discharge and low wind conditions enabled undisturbed development of the bulge. The ideal model simulation

1 | showed that the bulge continued to develop steadily for at least 10 rotation periods. Horner-Devine  
2 | [et al.](#) (2006) argues that in the case of high inflow, i.e. large Froude number,  $Fr = U(g'H)^{-1/2}$ ,  
3 | where  $U = Q(HW)^{-1}$ ,  $W$  is river width and  $H$  is river depth, the plume becomes unstable after 5-6  
4 | rotation periods. In our case, the Froude number stayed between 0.9 and 1.5 during the whole mod-  
5 | elling period ( $W = 700$  m,  $H = 7$  m). The plume was also stable in the numerical experiments of Nof  
6 | & Pichevin (2001) and Fong & Geyer (2002).

7 |  
8 | We estimated the movement of the bulge centre in the ideal simulation. The bulge centre moved  
9 | steadily to the north, completing about 8 km during nine rotation periods (Fig. [810a](#)). As the centre  
10 | also moved downstream actual offshore reach of the centre was 6 km. The radius of the ideal bulge  
11 | increased from 4 to 9 km from 0.5T to 10T. Thus, by the end of our simulation the ratio of bulge  
12 | centre,  $y_c$ , to bulge radius was less than 0.7, which according to Horner-Devine [et al.](#) (2006) means  
13 | that the bulge does not separate from the wall and flow into the coastal current does not decrease.  
14 | The latter was evident from our numerical simulation with the ideal bulge.

15 |  
16 | The movement of the real bulge centre was more “chaotic” (Fig. [108b](#)). At each one-hour timestep,  
17 | the bulge centre was defined if the anti-cyclonic circulation with closed streamlines existed (i.e. Fig.  
18 | [34k](#)). When ambient current overrode bulge circulation, the bulge centre was not defined (i.e. Fig.  
19 | [34i](#)), although the bulge still existed if we look at the distribution of the tracer concentration. Thus,  
20 | the movement of the bulge centre was not followed continuously. The main feature in the move-  
21 | ment of the bulge centre was offshore-onshore oscillations (Fig. [810b](#)). This behaviour is somewhat  
22 | similar to bulge pinch-off described by Horner-Devine [et al.](#) (2006). Horner-Devine [et al.](#) (2006)  
23 | proposed the ratio of internal radius,  $L_i = U / f$ , to bulge Rossby radius,  $L^* = L_i / L_b$ , to estimate  
24 | bulge behaviour. In the case of the Daugava discharge, that ratio was between 0.81-1.26, which cor-  
25 | responds to situations where the bulge is forced offshore relative to its radius (Horner-Devine [et al.](#);  
26 | 2006, Fig. 17d-g). In the case of a high Froude number and/or low  $g'$  (in our case  $0.045 \text{ m s}^{-2}$ ), the  
27 | bulge becomes unstable and the flow to the coastal current is reduced (Horner-Devine [et al.](#) 2006).  
28 | The behaviour of the Daugava river bulge from satellite images and the real numerical model simu-  
29 | lation (Fig. [34](#)) showed that river water was mainly contained in the bulge and there were numerous  
30 | intrusions at the outer perimeter of the bulge, which is qualitatively similar to the bulge behaviour  
31 | in the model simulation by Horner-Devine [et al.](#) (2006, his Fig. 14).

32 |

1 Horner-Devine et al. (2015) summarise the results of the volume fraction going into a coastal cur-  
2 rent ~~current~~ relative to river discharge, depending on inflow Rossby number. A relatively high  
3 Rossby number  $O [1]$  implies that most freshwater stays in the bulge while a lower Rossby number  
4 would imply that there is less water going into the bulge and more into the coastal current. In the  
5 Daugava River outflow, the inflow Rossby number varied between 3.4 and 5.7, which suggests that  
6 almost all of the river water should have been trapped in the bulge. Our estimates from the numeri-  
7 cal model calculation showed that the fraction of river water that formed a coastal current was up to  
8 ten times smaller than the amount of river water that remained in the bulge. In the ideal case, con-  
9 siderable volume went into the coastal current, although the  $Q$ ,  $Fr$ ,  $Ro$  and  $g'$  were the same for  
10 ideal and real model simulations.

11

12 The explanation of the discrepancy between the ideal bulge and laboratory experiments could be the  
13 different behaviour of the plume in a near-field region. In a near-field region, river flow has a lift off  
14 point in the location where river water detaches from the bottom and the upper layer Froude number  
15 is equal to one (Horner-Devine et al., 2015). At the lift off point, vertical velocities cause shoaling  
16 of the plume interface and acceleration of the upper layer flow at a more seaward region. This, in  
17 turn, increases the Froude number, resulting in intense vertical mixing. In our idealized numerical  
18 simulation, the lift off occurred at about 0.5 km from the river mouth (Fig. 68a). The most intensive  
19 mixing started at ~~one-1~~ km from the coast where tracer concentrations were below the limit of the  
20 bulge definition (white area in Fig. 68a and low tracer concentration in Fig 45a). The intensive mix-  
21 ing suppressed horizontal flow and the current velocities were low right behind the intense mixing  
22 zone, while the current velocities were higher at the left and right side of the mixing zone (Fig.  
23 68a). Thus, the intensive mixing zone created a barrier for the river water flow and splitted it into  
24 two jets. The jet on the right formed a rotating bulge. As the barrier altered the flow direction, the  
25 flow angle was notably smaller than 90 degrees, resulting in a bulge centre located closer to the  
26 coast (Avicola and Huq, 2003b). The jet on the left remained on the outer edge of the bulge. Such a  
27 barrier region is not observed in laboratory simulations. Natural buoyant river plumes have a small  
28 vertical to horizontal aspect ratio,  $O [10^{-3}]$ , where vertical turbulent flux of density is considered to  
29 be dominant over horizontal turbulent fluxes (Horner-Devine et al., 2015). For laboratory simula-  
30 tions, the aspect ratio is at least an order of magnitude smaller. Horizontal turbulence flux would be  
31 comparable in magnitude with vertical mixing and a sharply separated region of intense mixing is  
32 far less likely to form. In addition, in our numerical simulations, the Daugava River runoff was  
33 smeared over 5 horizontal grid points right at the coast, which enables a better resolution of the  
34 river plume in the near field than, for instance, achieved by Hetland (2005).

1

2 In the case of the realistic model simulation, wind mixing overpowered the local mixing, therefore  
3 avoiding creation of the barrier region. The density-driven [and wind forced](#) background currents  
4 restricted the development of a plume coastal current and pushed the river bulge offshore. As a re-  
5 sult, the bulge centre was further away from the coast (see Fig. [108b](#)).

6

## 7 **5 Conclusions**

8 Satellite TSM images showed a clearly formed river bulge from the Daugava River discharge dur-  
9 ing the studied low wind period. Satellite images also confirmed anti-cyclonic rotation inside the  
10 bulge. The bulge grew up to 20 km in diameter before being diluted. A high-resolution numerical  
11 model simulation repeated the plume behaviour satisfactorily and enabled a detailed study of the  
12 bulge dynamics. While previous studies conclude that balance in equation (23) is valid for the  
13 bulge, our study showed that geostrophic balance is valid for the entire mid-field of the bulge [ex-](#)  
14 [cept during 1-1.5T at the beginning of the bulge formation](#). Comparison of realistic and idealized  
15 model simulations showed a significant effect of wind-driven and density-driven circulation in the  
16 evolution of the river bulge, even if the wind speed was moderate.

17

18 The bulge radius was non-dimensionalized with the bulge Rossby radius. The [real model simulation](#)  
19 [\(measured wind and realistic ambient density\) satellite remote sensing](#) and [the](#) ideal simulation with  
20 no wind and uniform ambient density gave  $r_b \sim t^{0.50 \pm 0.04}$  and  $r_b \sim t^{0.28 \pm 0.01}$ , with the coefficients of de-  
21 termination being  $R^2=0.90$  and  $R^2=0.98$ , respectively. ~~gave the growth of the non-dimensional~~  
22 ~~bulge radius as  $r_b \sim t^{0.31 \pm 0.23}$  and  $r_b \sim t^{0.28 \pm 0.01}$ , with the coefficient of determination being  $R^2=0.87$  and~~  
23  ~~$R^2=0.98$  respectively. In the real model simulation (measured wind and realistic ambient density),~~  
24 ~~the  $r_b \sim t^{0.50 \pm 0.04}$  ( $R^2=0.90$ ).~~ The bulge spreading rates agree well with laboratory experiments ( $\sim t^{1/4}$  by  
25 Horner-Devine [et al.](#) (2006)) and fit in the margin of the Niagara River bulge study ( $\sim t^{0.46 \pm 0.29}$  by  
26 Horner-Devine et al. (2008)).

27

28 Mean depth and radius as well as the volume were larger for the realistic model bulge than for the  
29 idealized bulge. River bulge behaviour from satellite images and the real numerical model simula-  
30 tion showed that river water is mainly contained in the bulge and there were numerous intrusions at  
31 the outer perimeter of the bulge [due to caused by prevailing upwelling favourable and onshore](#)

1 | [winds](#). The fraction of river water that formed a coastal current was up to ten times smaller than the  
2 | amount of river water that remained in the bulge.

3 |  
4 | In the ideal simulation, considerable volume went into the coastal current, although the  $Q$ ,  $Fr$ ,  $Ro$   
5 | and  $g'$  were the same for ideal and real model simulations. The ideal numerical model simulation  
6 | showed that in the case of high inflow Rossby number the river inflow might split into two jets in  
7 | the plume near field region, with a strong mixing zone in-between. Although the ideal and real  
8 | bulges were similar, ~~the splitting of the outflow into two jets caused~~ the bulge centre ~~was to be~~  
9 | closer to the coast in the case of the ideal bulge than in the case of the real bulge ~~due to splitting of~~  
10 | ~~the outflow into two jets~~.

### 13 | **Acknowledgement**

14 | Volume flux data for Gauja and Lielupe rivers were provided by state limited Liability Company  
15 | “Latvian Environment, Geology and Meteorology Centre” in Riga, Latvia. Volume flux data for  
16 | river Daugava was provided by "Latvenergo AS" (State joint stock Company that provides electric-  
17 | ity for the country's citizens). [The work was financially supported by institutional research funding](#)  
18 | [IUT \(19-6\) of the Estonian Ministry of Education and Research](#).

## 1 **References**

- 2 Arakawa, A. and Lamb, V. R.: Computational design of the basic dynamical processes of the UCLA  
3 General Circulation Model. *Meth. Comput. Phys.*, 173-263, 1977.
- 4 Attila, J., Koponen, S., Kallio, K., Lindfors, A., Kaitala, S., and Ylöstalo, P.: MERIS Case II water  
5 processor comparison on coastal sites of the northern Baltic Sea. *Remote Sensing of Environment*,  
6 128, 138-149, 2013.
- 7 Avicola, G., and Huq, P.: The characteristics of the recirculating bulge region in coastal buoyant  
8 outflows. *Journal of Marine Research*, 61(4), 435-463(29), 2003.
- 9 [BSHC \(Baltic Sea Hydrographic Commission\): Baltic Sea Bathymetry Database version 0.9.3.](#)  
10 Downloaded from <http://data.bshc.pro/> on 28.02.2014, 2013
- 11 [Beltrán-Abaunza, J. M., Kratzer, S., and Brockmann, C.: Evaluation of MERIS products from](#)  
12 [Baltic Sea coastal waters rich in CDOM. \*Ocean Sci.\*, 10, 377-396, doi:10.5194/os-10-377-2014,](#)  
13 [2014.](#)
- 14 Burchard, H. and Bolding, K.: GETM - a general estuarine transport model. Scientific  
15 documentation. Technical Report EUR 20253 EN, European Commission, 2002.
- 16 Burchard, H. and Rennau, H.: Comparative quantification of physically and numerically induced  
17 mixing in ocean models. *Ocean Modelling*, 20 (3), 293–311, 2008.
- 18 Chant, R. J., Wilkin, J., Zhang, W., Choi, B.-J., Hunter, E., Castelao, R., Glenn, S., Jurisa, J.,  
19 Schofield, O., Houghton, R., Kohut, J., Frazer, T.K., and Moline, M.A.: Dispersal of the Hudson  
20 River plume in the New York Bight: Synthesis of observational and numerical studies during  
21 LaTTE. *Oceanography*, 21(4), 148-161, 2008.
- 22 Dee, D.P., Uppala, S.M., Simmons, A.J., Berrisford, P., Poli, P., Kobayashi, S., Andrae, U.,  
23 Balmaseda, M.A., Balsamo, G., Bauer, P., Bechtold, P., Beljaars, A.C.M., van de Berg, L., Bidlot, J.,  
24 Bormann, N., Delsol, C., Dragani, R., Fuentes, M., Geer, A.J., Haimberger, L., Healy, S.B.,  
25 Hersbach, H., Holm, E.V., Isaksen, L., Kallberg, P., Köhler, M., Matricardi, M., McNally, A.P.,  
26 Monge-Sanz, B.M., Morcrette, J.-J., Park, B.-K., Peubey, C., de Rosnay, P., Tavolato, C., Thepaut, J.-  
27 N., and Vitart, F.: The ERA-Interim reanalysis: configuration and performance of the data  
28 assimilation system. *Q. J. Roy. Meteor. Soc.*, 137, 553–597, 2011.
- 29 [Doerffer, R., Sorensen K. and Aiken, J.: MERIS potential for coastal zone applications,](#)  
30 [International Journal of Remote Sensing 20 \(9\), 1809–1818, 1999.](#)
- 31 Doerffer, R. and Schiller, H.: The MERIS case 2 water algorithm. *International Journal of Remote*  
32 *Sensing*, 28(3-4), 517–535, 2007.

1 [Doerffer, R. and Schiller, H. MERIS Regional Coastal and Lake Case 2 Water Project atmospheric](#)  
2 [correction ATBD \(Algorithm Theoretical Basis Document\). 1.0. 41 pp. 2008.](#)

Formatted: Space Before: 0 pt

3  
4 Dzwonkowski, B. and Yan, X.: Tracking of a Chesapeake Bay estuarine outflow plume with  
5 satellite-based ocean color data. *Continental Shelf Research*, 25(16), 1942-1958, 2005.

6 Fernández-Nóvoa, D., Mendes, R., Decastro, M., Dias, J., Sánchez-Arcilla, A., and Gómez-  
7 Gesteira, M.: Analysis of the influence of river discharge and wind on the Ebro turbid plume using  
8 MODIS-Aqua and MODIS-Terra data. *Journal of Marine Systems*, 142, 40-46, 2015.

9 Fong, D.A. and Geyer, W.R.: The Alongshore Transport of Freshwater in a Surface-Trapped River  
10 Plume. *J. Phys. Oceanog.*, 32, 957-972, 2002.

11 [Funkquist, L. and Kleine, E.: An introduction to HIROMB, an operational baroclinic model for the](#)  
12 [Baltic Sea. Tech. Rep. SMHI., Norrköping, 2000.](#)

Formatted: Space Before: 0 pt

13 [Gitelson, A. A., Gurlin, D., Moses, W.J. and Barrow, T.: A bio-optical algorithm for the remote](#)  
14 [estimation of the chlorophyll-a concentration in case 2 waters. Environmental Research Letters](#)  
15 [4\(4\), Article Number: 045003 DOI:10.1088/1748-9326/4/4/045003, 2009.](#)

Formatted: English (United Kingdom)

16 [Goyens, C., Jamet, C. and Schroeder, T.: Evaluation of four atmospheric correction algorithms for](#)  
17 [MODIS-Aqua images over contrasted coastal waters. Remote Sens. Environ., 131, 63-75, 2013](#)

18 Gräwe, U., Holtermann, P., Klingbeil, K. and Burchard, H.: Advantages of vertically adaptive  
19 coordinates in numerical models of stratified shelf seas. *Ocean Model.*, 92, 56-68, 2015.

20 [Gregorio, S.O., Haidvogel, D.B., Thomasa, P.J., Taskinoglu, E.S. and Skeend, A.J.: Laboratory](#)  
21 [and numerical simulations of gravity-driven coastal currents: Departures from geostrophic theory.](#)  
22 [Dynamics of Atmospheres and Oceans 52 \(2011\) 20– 50, 2011.](#)

23 Hetland, R.D. and Signell, R.P.: Modelling coastal current transport in the Gulf of Maine. *Deep-Sea*  
24 *Res. II*, 52, 2430-2449, 2005.

25 Hopkins, J., Lucas, M., Dufau, C., Sutton, M., Stum, J., Lauret, O., and Channelliere, C., 2013.  
26 Detection and variability of the Congo River plume from satellite derived sea surface temperature,  
27 salinity, ocean colour and sea level. *Remote Sensing of Environment*, 139, 365-385, 2013.

28 Horner-Devine, A.R., [Fong, D. A., Monismith, S. G. and Maxworthy, T.:](#) [Laboratory experiments](#)  
29 [simulating a coastal river inflow. J. Fluid Mech. 555, 203-232, 2006.](#)

30 [Velocity, density, and transport measurements in rotating, stratified flows. Experiments in Fluids](#)  
31 [online, 1-13, 2006.](#)

- 1 Horner-Devine, A.R., Fong, D.A., and Monismith, S.G.: Evidence for the inherent unsteadiness of a  
2 river plume: Satellite observations of the Niagara River discharge., *Limnol. Oceanogr.*, 53, 2731-  
3 2737, 2008.
- 4 Horner-Devine, A.R.: The bulge circulation in the Columbia River plume., *Cont. Shelf Res.*, 29,  
5 234-251, 2009.
- 6 Horner-Devine, A.R., Hetland, R., and Macdonald, D.: Mixing and Transport in Coastal River  
7 Plumes. *Annual Review of Fluid Mechanics*, 47, 569-594, 2015.
- 8 Keruss, M. and Sennikovs, J.: Determination of tides in Gulf of Riga and Baltic Sea. *Proc.*  
9 *International Scientific Colloquium 'Modelling of Material Processing'*, Riga, May 28 - 29, 1999.
- 10 Klingbeil, K., Mohammadi-Aragh, M., Gräwe, U., and Burchard, H. Quantification of spurious  
11 dissipation and mixing discrete variance decay in a finite-volume frame- work. *Ocean Model.* 81,  
12 49–64, 2014.
- 13 Kudela, R. M., Horner-Devine, A. R., Banas, N. S., Hickey, B. M., Peterson, T. D., Lessard, E. J.,  
14 Frame, E., Bruland, K.W., Lohan ,M., Jay, D. A., Peterson, J., Peterson, B., Kosro, M., Palacios,  
15 S., and Dever, E.P.: Multiple trophic levels fueled by recirculation in the Columbia River plume.  
16 *Geophys. Res. Lett.*, 37, 7, 2010.
- 17 [Lips, U., Zhurbas, V., Skudra, M. and Väli, G. A numerical study of circulation in the Gulf of Riga,](#)  
18 [Baltic Sea. Part I: Whole-basin gyres and mean currents. \*Cont. Shelf Res.\*, 112, 1-13, 2016.](#)
- 19 Maljutenko, I. and Raudsepp, U.: Validation of GETM model simulated long-term salinity fields in  
20 the pathway of saltwater transport in response to the Major Baltic Inflows in the Baltic Sea.  
21 *IEEE/OES Baltic International Symposium (BALTIC)*, 2014.
- 22 Mendes, R., Vaz, N., Fernández-Nóvoa, D., Silva, J., Decastro, M., Gómez-Gesteira, M., and Dias,  
23 J.: Observation of a turbid plume using MODIS imagery: The case of Douro estuary (Portugal).  
24 *Remote Sensing of Environment*, 154, 127-138, 2014.
- 25 Nof, D., and Pichevin, T.: The Ballooning of Outflows. *J. Phys. Oceanogr.* 31(10), 3045-3058,  
26 2001.
- 27 Pan, J., Gu, Y., and Wang, D.: Observations and numerical modeling of the Pearl River plume in  
28 summer season. *J. Geophys. Res.: Oceans*, 119(4), 2480-2500, 2014.
- 29 Pietrzak, J.: The use of TVD limiters for forward-in-time upstream-biased advection schemes in  
30 ocean modeling, *Mon. Weather Rev.*, 126, 812–830, 1998.
- 31 [Raudsepp, U. Interannual and seasonal temperature and salinity variations in the Gulf of Riga and](#)  
32 [corresponding saline water inflow from the Baltic Proper. \*Nordic Hydrology\*, 32 \(2\), 135–160.](#)

Formatted: Space Before: 0 pt

1 [2001.](#)  
2 [Raudsepp, U., Beletsky, D. and Schwab, D. J. Basin-scale topographic waves in the Gulf of Riga.](#)  
3 [Journal of Physical Oceanography, 33, 1129–1140, 2003.](#)  
4 Saldías, G., Sobarzo, M., Largier, J., Moffat, C., and Letelier, R.: Seasonal variability of turbid river  
5 plumes off central Chile based on high-resolution MODIS imagery. Remote Sensing of  
6 Environment, 123, 220-233, 2012.  
7 Shchepetkin, A.F. and McWilliams, J.C.: A method for computing horizontal pressuregradient force  
8 in an oceanic model with a nonaligned vertical coordinate. J. Geophys. Res. 108, 2003.  
9 Siitam, L., Sipelgas, L., and Uiboupin, R.: Analysis of natural background and dredging-induced  
10 changes in TSM concentration from MERIS images near commercial harbours in the Estonian  
11 coastal sea. International Journal of Remote Sensing, 35(18), 6764 - 6780, 2014.  
12 Stips, A., Bolding, K., Pohlmann, T., and Burchard, H.: Simulating the temporal and spatial  
13 dynamics of the North Sea using the new model GETM (general estuarine transport model. Ocean  
14 Dyn. 54 (2), 266-283, 2004.  
15 [Soosaar, E., Hetland, R. D., Horner-Devine, A., Avenor, M. E. and Raudsepp, U.: Offshore](#)  
16 [spreading of buoyant bulge from numerical simulations and laboratory experiments. In: IEEE](#)  
17 [Xplore: Baltic International Symposium \(BALTIC\), 2014 IEEE/OES, 27-29 May 2014, Tallinn](#)  
18 [Estonia. IEEE., 2014](#)  
19 [Soosaar, E., Maljutenko, I., Raudsepp, U., and Elken, J. An investigation of anticyclonic circulation](#)  
20 [in the southern Gulf of Riga during the spring period. Cont. Shelf Res., 78, 75-84, 2014.](#)  
21 Thomas, P.J. and Linden, P.F.: Rotating gravity currents: small-scale and large-scale laboratory  
22 experiments and a geostrophic model. J. Fluid Mech., 578, 35-65, 2007.  
23 Umlauf, L. and Burchard, H.: Second-order turbulence closure models for geophysical boundary  
24 layers. A review of recent work. Cont. Shelf Res. 2, 795–827, 2005.  
25 [Undén, P., Rontu, L., Jörvinen, H., Lynch, P., Calvo, J., Cats, G., Cuxart, J., Eerola, K., Fortelius,](#)  
26 [C., Garcia-Moya, J.A., Jones, C., Lenderink, G., McDonald, A., McGrath, R., Navascues, B.,](#)  
27 [Nielsen, N.W., Ødegaard, V., Rodrigues, E., Rummukainen, M., Rõõm, R., Sattler, K., Sass, B.H.,](#)  
28 [Savijörvi, H., Schreur, B.W., Sigg, R., The, H., Tjmm, A.:HIRLAM-5 scientific documentation,](#)  
29 <http://www.hirlam.org/>, 2002.  
30 [Vaičiūtė, D., Bresciani, M. and Bučas, M.: Validation of MERIS Bio-Optical Products with In Situ](#)  
31 [Data in the Turbid Lithuanian Baltic Sea Coastal Waters. Journal of Applied Remote Sensing 6:](#)  
32 [063568-1–063568-20. doi:10.1117/1.JRS.6.063568, 2012.](#)

Formatted: Space Before: 0 pt

Formatted: English (United Kingdom)

Field Code Changed

1 Valente, A., and Silva, J.: On the observability of the fortnightly cycle of the Tagus estuary turbid  
2 plume using MODIS ocean colour images. *Journal of Marine Systems*, 75(1-2), 131-137, 2009.

3 Whitney, M., and Garvine, R.: Wind influence on a coastal buoyant outflow. *J. Geophys. Res.*,  
4 110(C3), 2005.

5 Yankovsky, A.E. and Chapman, D.C.: A simple theory for the fate of buoyant coastal discharges. *J.*  
6 *of Phys. Oceanogr.*, 27, 1386-1401, 1997.

7

### 8 **Figure captions**

9

10 Figure 1. Map showing the location of the Gulf of Riga in the Baltic Sea (a). Embedded are mean  
11 (bold) temperature (dashed) and salinity (dash dotted) profiles with standard deviations (thin) from  
12 the central Gulf of Riga (adopted from Raudsepp, 2001). Topography of the Gulf of Riga (b). Ar-  
13 rows mark river mouth locations for the Daugava (D), Lielupe (L) and Gauja (G) rivers. The square  
14 shows the location of the weather station. Bold dashed line shows the transect of ferry-box meas-  
15 urements used for the model validation.

16

17 Figure 2. Time series of daily mean Daugava River discharge (a), hourly wind speed (b) and wind  
18 direction (c) measured at Ruhnu weather station. Black dots show time instants when satellite im-  
19 ages were acquired. The gray area marks the period between the first and last available satellite im-  
20 age from the study period (March 20 to April 4).

21

22 Figure 3. Time series of (a) daily mean Daugava River discharge; (b) 3-hour wind speed (bold), east  
23 (solid) and north (dashed) wind components from the HIRLAM-ETA dataset at Ruhnu Island, and 3  
24  $\text{m s}^{-1}$  wind speed (dash dotted); c) offshore location of the maximum salinity gradient from model  
25 (solid) and ship measurements (open square) for the period from 20 March to 5 April 2014. Dis-  
26 tance is measured along the ship track from the mouth of the Daugava River.

27

28 Figure 4. TSM concentration maps for the southern part of the Gulf of Riga from satellite images  
29 (left column) and TSM concentration and surface velocity maps from the numerical simulation  
30 (right column). Bold contour on satellite images shows the indicative edge of the Daugava River  
31 bulge. Black contours on the numerical model simulation maps represent TSM concentrations of  
32  $\log_{10}(\text{TSM})=-0.15$  and  $=-0.05$ . The former is used for the determination of the Daugava River bulge.  
33 The coordinate system is on the UTM-34v projection. (*Cont*)

34

1 Figure 5. Instantaneous surface velocity and TSM concentration maps for simulation with realistic  
2 ambient density and no wind forcing (a) and idealized model simulation with uniform ambient den-  
3 sity and no wind forcing (b) at noon on 29 March 2007. Solid lines represent TSM concentrations of  
4  $\log_{10}(\text{TSM})=-0.15$  and  $=-0.05$ . The coordinate system is on the UTM-34v projection.

5

6 Figure 6. Instantaneous surface TSM concentration maps for simulation with uniform ambient den-  
7 sity and a constant wind speed of  $4 \text{ m s}^{-1}$  blowing in a downstream (a), upstream (b), offshore (c)  
8 and onshore (d) direction at 6T from the start of the simulation. Solid lines represent TSM concen-  
9 trations of  $\log_{10}(\text{TSM})=-0.15$  and  $=-0.05$ . The coordinate system is on the UTM-34v projection.

10

11 Figure 7. Time series of the Daugava River bulge mean depth (a), bulge radius (b), bulge volume (c)  
12 and the bulge effective radius scaled with bulge Rossby radius (d). The solid line represents the real  
13 model simulation and the dash-dotted line the idealized model simulation. Time series of the bulge  
14 radius where bulge is defined  $I=\log_{10}(\text{TSM})>-0.05; -0.10; -0.20; -0.25$  (dotted) (b). Time series of  
15 cumulative river water (dashed), bulge volume (black) and volume of the coastal current (red) in the  
16 real model simulation (solid) and ideal model simulation (dash-dotted) (c). Triangles represent the  
17 rotation period of the earth starting from 24 March 2007 05:00.

18

19 Figure 8. Bulge depth and depth averaged velocities, the terms ( $T_1$ ,  $T_2$ ,  $T_3$ ) of the balance (see Eq.  
20 (3)) and the combinations of the terms for idealized (left column) and realistic (right column) model  
21 simulations on 29 March 2007 at 20:00. Bulge depth and depth averaged velocities (a-b), centrifu-  
22 gal term ( $T_1$ ) (c-d), Coriolis term ( $T_2$ ) (e-f), pressure gradient term ( $T_3$ ) (g-h),  $T_1+T_2$  (i-j),  $T_1-T_2$  (k-  
23 l),  $T_2-T_3$  (m-n) and  $T_1+T_2-T_3$  (o-p). The contour interval is  $1 \text{ m s}^{-2}$ . The red isoline represents zero.  
24 The blank area within the bulge is where the tracer concentrations were below the threshold values  
25 of the bulge definition (see text for bulge definition). The origin of the coordinate system is at the  
26 mouth of the Daugava River. True north is shown with the arrow. (Cont.)

27

28 Figure 9. Time series of spatially averaged momentum balance terms (see Eq. (3)): centrifugal term  
29 ( $T_1$ ) (solid), Coriolis term ( $T_2$ ) (dashed), pressure gradient term ( $T_3$ ) (dash dotted) for ideal (a) and  
30 real bulge (b). Triangles represent the rotation period of the earth starting from 24 March 2007  
31 05:00.

32

33 Figure 10. The trajectories of the bulge centre for the idealized simulation (a) and the realistic simu-  
34 lation (b) from 24 March 2007 05:00 to 5 April 2007 00:00. Each dot shows the location of the  
35 bulge centre at hourly intervals. Dashed lines show the normal and tangent to the coastline, distance

1 of the bulge centre from the location at 1T up to the end of the simulation, the distance of the bulge  
2 centre at the end of the simulation to the coast in the direction of the normal to the coast. 1T and 4T  
3 show the location of the bulge centre after one and four rotation periods of the earth starting from  
4 24 March 2007 05:00 (a). Discontinuities in the bulge trajectories for the realistic model simulation  
5 exist because the bulge centre was defined only if anti-cyclonic circulation with closed streamlines  
6 was present (b).

7

8